Inorg. Chem. **XXXX**, *XX*,

Inorganic Chemistry
Article

High-Nuclearity Ce/Mn and Th/Mn Cluster Chemistry: Preparation of Complexes with $[Ce_4Mn_{10}O_{10}(OMe)_6]^{18+}$ and $[Th_6Mn_{10}O_{22}(OH)_2]^{18+}$ Cores

Abhudaya Mishra,[†] Anastasios J. Tasiopoulos,[†] Wolfgang Wernsdorfer,[‡] Khalil A. Abboud,[†] and George Christou*,[†]

Department of Chemistry, University of Florida, Gainesville, Florida 32611-7200, and Laboratoire Louis Néel-CNRS, BP 166, 25 Avenue des Martyrs, 38042 Grenoble, Cedex 9, France

Received October 11, 2006

The syntheses, structures, and magnetic properties are reported of the mixed-metal complexes $[Ce_4Mn_{10}O_{10}(OMe)_6(O_2CPh)_{16}(NO_3)_2(MeOH)_2(H_2O)_2]$ (**1**) and $[Th_6Mn_{10}O_{22}(OH)_2(O_2CPh)_{16}(NO_3)_2(H_2O)_8]$ (**2**), which were both prepared by the reaction of $(NBu^n_4)[Mn_4O_2(O_2CPh)_9(H_2O)]$ (**3**) with a source of the heterometal in MeCN/MeOH. Complexes **1** and **2** crystallize in the monoclinic space group $C2/c$ and the triclinic space group $P\bar{1}$, respectively. Complex **1** consists of 10 Mn^{III}, 2 Ce^{III}, and 2 Ce^{IV} atoms and possesses a very unusual tubular $[Ce_4Mn_{10}O_{10}(OMe)_6]^{18+}$ core. Complex **2** consists of 10 Mn^{IV} and 6 Th^{IV} atoms and possesses a $[Th_6Mn_{10}O_{22}(OH)_2]^{18+}$ core with the metal atoms arranged in layers with a 2:3:6:3:2 pattern. Peripheral ligation around the cores is provided by 16 bridging benzoates, 2 chelating nitrates, and either (i) 2 each of terminal H_2O and MeOH groups in **1** or (ii) 8 terminal H_2O groups in **2**. Complex **1** is the largest mixed-metal Ce/Mn cluster and the first 3d/4f cluster with mixed-valency in its lanthanide component, while complex **2** is the first Th/Mn cluster and the largest mixed transition metal/actinide cluster to date. Solid-state dc and ac magnetic susceptibility measurements on **1** and **2** establish that they possess $S = 4$ and 3 ground states, respectively. Ac susceptibility studies on **1** revealed nonzero frequency-dependent out-of-phase (χ_M'') signals at temperatures below 3 K; complex **2** displays no χ_M'' signals. However, single-crystal magnetization vs dc field scans at variable temperatures and variable sweep-rates down to 0.04 K on **1** revealed no noticeable hysteresis loops, except very minor ones at 0.04 K assignable to weak intermolecular interactions propagated by hydrogen bonds involving Ce^{III}-bound ligands. Complex **1** is thus concluded not to be a single-molecule magnet (SMM), and the combined results thus represent a caveat against taking such ac signals as sufficient proof of a SMM.

Introduction

High-nuclearity transition metal cluster chemistry has been attracting intense interest during the last several years. This is due to the combination of the aesthetically pleasing structures that many such molecular clusters possess and the often unusual and even novel magnetic properties that some of them display. In particular, some of these clusters have been found to be single-molecule magnets (SMMs), which are individual molecules capable of functioning as nanoscale magnetic particles and which thus represent a molecular approach to nanomagnetism.[1] Such molecules behave as magnets below their blocking temperature (T_B), exhibiting hysteresis in magnetization versus dc field scans. These hysteresis loops display increasing coercivity with decreasing temperature and increasing field sweep rates, the characteristic signature of superparamagnets. This magnetic behavior of SMMs results from the combination of a large ground spin state (S) with a large and negative Ising (or easy-axis) type of magnetoanisotropy, as measured by the axial zero-field splitting parameter D.[1,2] In addition, there is extensive

* To whom correspondence should be addressed. Tel: +1-352-392-8314. Fax: +1-352-392-8757. E-mail: christou@chem.ufl.edu.
[†] University of Florida.
[‡] Laboratoire of Louis Néel-CNRS.

(1) (a) Christou, G.; Gatteschi, D.; Hendrickson, D. N., Sessoli, R. *MRS Bull.* **2000**, *25*, 66 and references therein. (b) Aromi, G.; Aubin, S. M. J.; Bolcar, M. A.; Christou, G.; Eppley, H. J.; Folting, K.; Hendrickson, D. N.; Huffman, J. C.; Squire, R. C.; Tsai, H.−L.; Wang, S.; Wemple, M. W. *Polyhedron* **1998**, *17*, 3005. (c) Christou, G. *Polyhedron* **2005**, *24*, 2065.
(2) (a) Sessoli, R.; Gatteschi, D.; Caneschi, A.; Novak, M. A. *Nature* **1993**, *365*, 141. (b) Sessoli, R.; Ysai, H. -L.; Schake, A. R.; Wang, S.; Vincent, J. B.; Folting, K.; Gatteschi, D.; Christou, G.; Hendrickson, D. N. *J. Am. Chem. Soc.* **1993**, *115*, 1804. (c) Thomas, L.; Lionti, L.; Ballou, R.; Gatteschi, D.; Sessoli, R.; Barbara, B. *Nature* **1996**, *383*, 145.

10.1021/ic061946y CCC: $37.00 © xxxx American Chemical Society
Published on Web 03/21/2007

bioinorganic interest in 3d metal clusters, and this includes Mn carboxylate clusters[3] because of their relevance to elucidating the nature and mechanism of action of the Mn_4-Ca core of the water oxidizing complex (WOC) of photosynthesis.[4]

In this paper, we report some recent progress in our ongoing program to develop high-nuclearity, mixed-metal cluster compounds involving 3d and 4f metals. As we shall describe, we have now also extended this work to a mixture of 3d and 5f metals for the first time. Most high-nuclearity, high-spin metal clusters are homometallic Mn species, as was the SMM prototype $[Mn_{12}O_{12}(O_2CMe)_{16}(H_2O)_4]$.[2,5] However, several groups,[6] as well as our own,[7−9] have more recently been exploring heterometallic 3d/4f species as a route to cluster compounds with interesting magnetic properties. Our own work has resulted in a number of new SMMs, namely Mn_8Ce,[7] $Mn_{11}Ln_4$,[8a] Mn_2Dy_2,[8b] and Fe_2Ln_2[9] clusters, although the Mn_8Ce SMM actually contains diamagnetic Ce^{IV}. In addition, both mixed 3d/4d and 3d/5d SMMs containing Mn are now known.[10]

The present results were obtained as part of our continuing efforts in Mn/Ce chemistry and have now led to a $Ce^{III}{}_2Ce^{IV}{}_2Mn^{III}{}_{10}$ product $[Ce_4Mn_{10}O_{10}(OMe)_6(O_2CPh)_{16}(NO_3)_2(MeOH)_2(H_2O)_2]$ (**1**) that is the first example of a Mn/Ce cluster to contain Ce^{III}. In addition, our previous results with Mn/Ce^{IV} made us wonder whether it might prove possible to extend this chemistry to a mixed 3d transition metal/actinide cluster, namely a Mn/Ac^{IV} (Ac = actinide) species. Indeed, we report the successful preparation of a $Th^{IV}{}_6Mn^{IV}{}_{10}$ complex $[Th_6Mn_{10}O_{22}(OH)_2(O_2CPh)_{16}(NO_3)_2(H_2O)_8]$ (**2**), which is the highest nuclearity mixed transition metal/actinide molecular complex to date. We herein describe the syntheses, crystal structures, and magnetic characterization of these species; portions of this work have been previously communicated.[11]

Experimental Section

Syntheses. All manipulations were performed under aerobic conditions using chemicals as received. $(NBu^n_4)[Mn_4O_2(O_2CPh)_9(H_2O)]$[12] (**3**) and $[Mn_3O(O_2CPh)_6(py)_2(H_2O)]$[13] (**4**) were prepared as previously reported.

$(NBu^n_4)_2Ce(NO_3)_6$. A solution of $(NH_4)_2Ce(NO_3)_6$ (15 g, 27 mmol) in H_2O (50 mL) was treated with a solution of NBu^n_4Br (18 g, 55 mmol) in H_2O (30 mL) to give a fine orange precipitate. The mixture was stirred for a few more minutes, filtered, and the solid washed with Et_2O and dried in vacuo. The yield was 90%.

$[Ce_4Mn_{10}O_{10}(OMe)_6(O_2CPh)_{16}(NO_3)_2(MeOH)_2(H_2O)_2]$ (1). Method A. A solution of complex **3** (1.0 g, 0.62 mmol) in MeCN (20 mL) was treated with solid $(NBu^n_4)_2Ce(NO_3)_6$ (0.98 g, 0.98 mmol) and was left stirring for 20 min. The resulting brown solution was filtered to remove an off-white precipitate, and the filtrate was then layered with MeOH (10 mL) and left undisturbed at room temperature. After ~2 weeks, the X-ray quality reddish-brown crystals of **1**·H_2O·4MeOH·6MeCN that had formed were collected by filtration, washed with Et_2O, and dried in vacuo; the yield was 25%. Dried crystals analyzed as **1**·$4H_2O$. Anal. Calcd (Found) for **1**·$4H_2O$ ($C_{120}H_{118}O_{62}N_2Mn_{10}Ce_4$): C, 39.06 (39.25); H, 3.22 (3.25); N, 0.76 (0.80) %. Selected IR data (KBr, cm^{-1}): 3408(s, br), 1599(s), 1556(s), 1449(w), 1385(s), 1025(w), 716(s), 676(m), 610(m, br), 563(m, br), 437(w).

Method B. Complex **1** can also be prepared by treating **4** (1.0 g, 0.92 mmol) in MeCN (20 mL) with solid $(NBu^n_4)_2Ce(NO_3)_6$ (0.91 g, 0.91 mmol) followed by stirring for 20 min. The subsequent workup was as described in Method A. The product was identified as **1**·$4H_2O$ by IR spectroscopy and elemental analysis. The yield was 20%. Anal. Calcd (Found) for **1**·$4H_2O$ ($C_{120}H_{118}O_{62}N_2Mn_{10}Ce_4$): C, 39.06 (39.21); H, 3.22 (3.20); N, 0.76 (0.78) %.

$[Th_6Mn_{10}O_{22}(OH)_2(O_2CPh)_{16}(NO_3)_2(H_2O)_8]$ (2). To a slurry of complex **3** (0.25 g, 0.16 mmol) in MeCN/MeOH (20/1 mL) was added solid $Th(NO_3)_4$·$3H_2O$ (0.17 g, 0.31 mmol), and the mixture was stirred for 30 min. The resulting brown solution was filtered and the filtrate concentrated by very slow evaporation. Dark red-brown crystals of **2**·10MeCN slowly grew over a few weeks, and these were collected by filtration, washed with acetone, and dried overnight in vacuo; the yield was 20%. Dried material analyzed as fully desolvated. Anal. Calcd (Found) for **2** ($C_{112}H_{98}O_{70}N_2Mn_{10}Th_6$): C, 29.67 (29.52); H, 2.18 (2.15); N, 0.62 (0.48) %. Selected IR data (KBr, cm^{-1}): 3392(s, br), 1598(m), 1522(s, br), 1448(w), 1384(s, br), 1025(w), 718(s), 685(m), 615(s, br), 571(w), 482(w).

X-ray Crystallography. Data were collected on a Siemens SMART PLATFORM equipped with a CCD area detector and a graphite monochromator utilizing Mo K_α radiation (λ = 0.71073 Å). Suitable crystals of the complexes were attached to glass fibers using silicone grease and transferred to a goniostat where they were cooled to 173 K for data collection. An initial search of reciprocal space revealed a monoclinic cell for **1** and a triclinic cell for **2**; the choice of space groups $C2/c$, and $P\bar{1}$, respectively, were confirmed by the subsequent solution and refinement of the structures. Cell

(3) (a) Mukhopadhyay, S.; Mandal, S. K.; Bhaduri, S.; Armstrong, W. H. *Chem. Rev.* **2004**, *104*, 3981. (b) Mishra, A.; Wernsdorfer, W.; Abboud, K. A.; Christou, G. *Chem. Commun.* **2005**, 54.

(4) (a) Loll, B.; Kern, J.; Saenger, W.; Zouni, A.; Biesiadka, J. *Nature* **2005**, *438*, 1040. (b) Ferreira, K. N.; Iverson, T. M.; Maghlaoui, K.; Barber, J.; Iwata, S. *Science* **2004**, *303*, 1831. (c) Yachandra, V. K.; Sauer, K.; Klein, M. P. *Chem. Rev.* **1996**, *96*, 2927.

(5) (a) Miyasaka, H.; Clérac, R.; Wernsdorfer, W.; Lecren, L.; Bonhomme, C.; Sugiura, K.; Yamashita, M. A. *Angew. Chem., Int. Ed.* **2004**, *43*, 2801. (b) Milios, C. J.; Raptopoulou, C. P.; Terzis, A.; Lloret, F.; Vicente, R.; Perlepes, S. P.; Escuer, A. *Angew. Chem., Int. Ed.* **2003**, *43*, 210. (c) Brechin, E. K.; Soler, M.; Davidson, J.; Hendrickson, D. N.; Parsons, S.; Christou, G. *Chem. Commun.* **2002**, 2252. (d) Price, D. J.; Batten, S. R.; Moubaraki B.; Murray, K. S. *Chem. Commun.* **2002**, 762. (e) Sanudo, E. C.; Wernsdorfer, W.; Abboud, K. A.; Christou, G. *Inorg. Chem.* **2004**, *43*, 4137. (f) Tasiopoulos, A. J.; Vinslava, A.; Wernsdorfer, W.; Abboud, K. A.; Christou, G. *Angew. Chem., Int. Ed.* **2004**, *43*, 2117. (g) Zaleski, C. M.; Depperman, E. C.; Dendrinou-Samara, C.; Alexiou, M.; Kampf, J. W.; Kessissoglou, D. P.; Kirk, M. L.; Pecoraro, V. L. *J. Am. Chem. Soc.* **2005**, *127*, 12862.

(6) (a) Osa, S.; Kido, T.; Matsumoto, N.; Re, N.; Pochaba, A.; Mrozinski, J. *J. Am. Chem. Soc.* **2004**, *126*, 420. (b) Zaleski, C. M.; Depperman, E. C.; Kampf, J. W.; Kirk, M. L.; Pecoraro, V. L. *Angew. Chem., Int. Ed.* **2004**, *43*, 3912. (c) Costes, J.-P.; Dahan, F.; Wernsdorfer, W. *Inorg. Chem.* **2006**, *45*, 5. (d) Mori, F.; Nyui, T.; Ishida, T.; Nogami,T.; Choi, K.; Nojiri, H. *J. Am. Chem. Soc.* **2006**, *128*, 1440.

(7) Tasiopoulos, A. J.; Wernsdorfer, W.; Moulton, B.; Zaworotko, M. J.; Christou, G. *J. Am. Chem. Soc.* **2003**, *125*, 15274.

(8) (a) Mishra, A.; Wernsdorfer, W.; Abboud, K. A.; Christou, G. *J. Am. Chem. Soc.* **2004**, *126*, 15648. (b) Mishra, A.; Wernsdorfer, W.; Parsons, S.; Christou, G.; Brechin, E. K. *Chem. Commun.* **2005**, 2086.

(9) Murugesu, M.; Mishra, A.; Wernsdorfer, W.; Abboud, K. A.; Christou, G. *Polyhedron*, **2006**, *25*, 613.

(10) (a) Sokol, J. J.; Hee, A. G.; Long, J. R. *J. Am. Chem. Soc.* **2002**, *124*, 7656. (b) Schelter, E. J.; Prosvirin, A. V.; Dunbar, K. R. *J. Am. Chem. Soc.* **2004**, *126*, 15004.

(11) Mishra, A.; Abboud, K. A.; Christou, G. *Inorg. Chem.* **2006**, *45*, 2364.

(12) Wemple, M. W.; Tsai, H.-L.; Wang, S.; Claude, J.-P.; Streib, W. E.; Huffman, J. C.; Hendrickson, D. N.; Christou, G. *Inorg. Chem.* **1996**, *35*, 6450.

(13) Vincent, J. B.; Chang, H. R.; Folting, K.; Huffman, J. C.; Christou, G.; Hendrickson, D. N. *J. Am. Chem. Soc.* **1987**, *109*, 5703.

Table 1. Crystallographic Data for **1**·H_2O·4MeOH·6MeCN and **2**·10MeCN

	1	**2**
formula	$C_{136}H_{146}N_8O_{63}Mn_{10}Ce_4$	$C_{132}H_{128}N_{12}O_{70}Mn_{10}Th_6$
fw, g/mol	4010	4944
space group	*C*2/*c*	$P\bar{1}$
a, Å	32.408(2)	15.0752(13)
b, Å	16.9687(11)	16.0141(14)
c, Å	27.6545(17)	17.8295(15)
α, deg	90	80.900(2)
β, deg	95.942(2)	72.585(2)
γ, deg	90	66.351(2)
V, Å^3	15126.2(17)	3758.5(6)
Z	4	1
T, K	173(2)	173(2)
radiation, Å[a]	0.71073	0.71073
ρ_{calc}, g/cm^3	1.750	2.183
μ, mm^{-1}	2.074	6.819
R1[b,c]	0.0805	0.0707
wR2[d]	0.1866	0.1647

[a] Graphite monochromator. [b] $I > 2\sigma(I)$. [c] $R1 = 100\sum(||F_o| - |F_c||)/\sum|F_o|$. [d] $wR2 = 100[\sum[w(F_o^2 - F_c^2)^2]/\sum[w(F_o^2)^2]]^{1/2}$, $w = 1/[\sigma^2(F_o^2) + [(ap)^2 + bp]$, where $p = [\max(F_o^2, O) + 2F_c^2]/3$.

parameters were refined using up to 8192 reflections. A full sphere of data (1850 frames) was collected using the *ω*-scan method (0.3° frame width). The first 50 frames were remeasured at the end of data collection to monitor instrument and crystal stability (maximum correction on *I* was <1 %). Absorption corrections by integration were applied based on measured indexed crystal faces. The structures were solved by direct methods in SHELXTL6,[14a] and refined on F^2 using full-matrix least-squares. The non-H atoms were treated anisotropically, whereas the hydrogen atoms were placed in calculated, ideal positions and refined as riding on their respective carbon atoms.

For **1**·H_2O·4MeOH·6MeCN, the unit cell consists of the cluster and both ordered (H_2O) and disordered (four MeOH and six MeCN) solvent molecules of crystallization. The contribution of the disordered solvents to the overall intensity data was removed using the program SQUEEZE,[14b] a part of the PLATON[14c] package of crystallographic software. One of the phenyl rings on C71 was disordered and was refined in two parts with site occupation factors dependently refined. A total of 858 parameters were included in the structure refinement on F^2 using 49 819 reflections with $I > 2\sigma(I)$ to yield R1 and wR2 of 8.05% and 18.66%, respectively.

For **2**·10MeCN, the asymmetric unit consists of half the cluster and five MeCN solvent molecules of crystallization. The latter were disordered and could not be modeled properly, and the program SQUEEZE[14b] was used to calculate the solvent disorder area and remove its contribution to the overall intensity data. A total of 791 parameters were included in the structure refinement on F^2 using 16 874 reflections with $I > 2\sigma(I)$ to yield R1 and wR2 of 7.07% and 16.47%, respectively.

Unit cell data and details of the structure refinements for **1**·H_2O·4MeOH·6MeCN and **2**·10MeCN are listed in Table 1.

Other Studies. Infrared spectra were recorded in the solid state (KBr pellets) on a Nicolet Nexus 670 FTIR spectrometer in the 400−4000 cm^{-1} range. Elemental analyses (C, H, and N) were performed by the in-house facilities of the University of Florida Chemistry Department. Variable-temperature dc and ac magnetic susceptibility data were collected at the University of Florida using a Quantum Design MPMS-XL SQUID susceptometer equipped with a 7 T magnet and operating in the 1.8−300 K range. Samples were embedded in solid eicosane to prevent torquing. Magnetization vs field and temperature data were fit using the program MAGNET.[15] Pascal's constants were used to estimate the diamagnetic correction, which was subtracted from the experimental susceptibility to give the molar paramagnetic susceptibility (χ_M). Studies at ultralow temperatures (<1.8 K) were performed on single crystals at Grenoble using an array of micro-SQUIDs.[16] The high sensitivity of this magnetometer allows the study of single crystals of the order of 10−500 μm; the field can be applied in any direction by separately driving three orthogonal coils.

Results and Discussion

Syntheses. High-nuclearity Mn clusters have previously been obtained by the reaction of preformed Mn_x clusters with bi-, tri-, or tetradentate (N/O) chelates.[17] Among the various Mn^{III} sources that have been explored, $(NBu^n_4)[Mn_4O_2(O_2CPh)_9(H_2O)]$ (**3**; $4Mn^{III}$) and $[Mn_3O(O_2CPh)_6(py)_2(H_2O)]$ (**4**; $2Mn^{III}$, Mn^{II}) have proven particularly effective, being found to often give higher nuclearity products. We also employed a modification of this strategy to access heterometallic species by treating complexes **3** or **4** with a heterometal salt, which allowed preparation of Mn/Ca and Mn/Ln^{III} (Ln = lantahanide) species.[3b,8a,9] Such reactions were carried out in a mixed solvent system such as MeCN/MeOH, which ensures solubility of all reactants and also can provide bridging MeO^- ligands. Hence, we employed the same general strategy in the present work with Ce^{IV} and Th^{IV}, but with one modification: for the Ce^{IV} reaction, more crystalline product was obtained by introducing the MeOH at the layering stage after the initial reaction had been carried out in MeCN. Several Mn/Ce(Th) ratios were explored, and we report only the ones that gave clean products. Thus, reaction of complex **3** with $(NBu^n_4)_2Ce(NO_3)_6$ in a 5:8 molar ratio led to subsequent isolation of complex **1**; the same product was obtained using complex **4**. The preparation of **1** is summarized in eq 1.

$$5[Mn_4O_2(O_2CPh)_9(H_2O)]^- + 8[Ce(NO_3)_6]^{2-} + 16MeOH + 9H_2O + 4e^- \rightarrow 13PhCO_2H + 19H^+ + 2[Ce_4Mn_{10}O_{10}(OMe)_6(O_2CPh)_{16}(NO_3)_2 - (MeOH)_2(H_2O)_2] + 44NO_3^- \quad (1)$$

A similar reaction was investigated with Th^{IV}, and this time the MeOH was needed in the reaction solution to help solubilize the $Th(NO_3)_4$·$3H_2O$ that was employed. Thus, reaction of complex **3** with $Th(NO_3)_4$·$3H_2O$ in a 5:12 molar ratio in MeCN/MeOH led to subsequent isolation of complex **2**. The same reaction but with an increased Mn^{III}_4/Th^{IV} ratio

(14) (a) Sheldrick, G. M. *SHELXTL6*; Bruker-AXS: Madison, WI, 2000. (b) van der Sluis, P.; Spek, A. L. *Acta Crystallogr*. **1990**, *A46*, 194. (c) Spek, A. L. *Acta Crystallogr*. **1990**, *A46*, C34.

(15) Davidson, E. R. *MAGNET*; Indiana University: Bloomington, IN.

(16) Wernsdorfer, W. *Adv. Chem. Phys*. **2001**, *118*, 99.

(17) (a) Brechin, E. K. *Chem. Commun.* **2005**, 5141. (b) Piligkos, S.; Rajaraman, G.; Soler, M.; Kirchner, N.; Slageren, J.; Bircher, R.; Parsons, S.; Gudel, H.-U.; Kortus, J.; Wernsdorfer, W.; Christou, G.; Brechin, E. K. *J. Am. Chem. Soc*. **2005**, *127*, 5572. (c) Boskovic, C.; Wernsdorfer, W.; Folting, K.; Huffman, J. C.; Hendrickson, D. N.; Christou, G. *Inorg. Chem.* **2002**, *41*, 5107. (d) Brechin, E. K.; Boskovic, C.; Wernsdorfer, W.; Yoo, J.; Yamaguchi, A.; Sanudo, E. C.; Concolino, T. R.; Rheingold, A. L.; Ishimoto, H.; Hendrickson, D. N.; Christou, G. *J. Am. Chem. Soc.* **2002**, *124*, 9710.

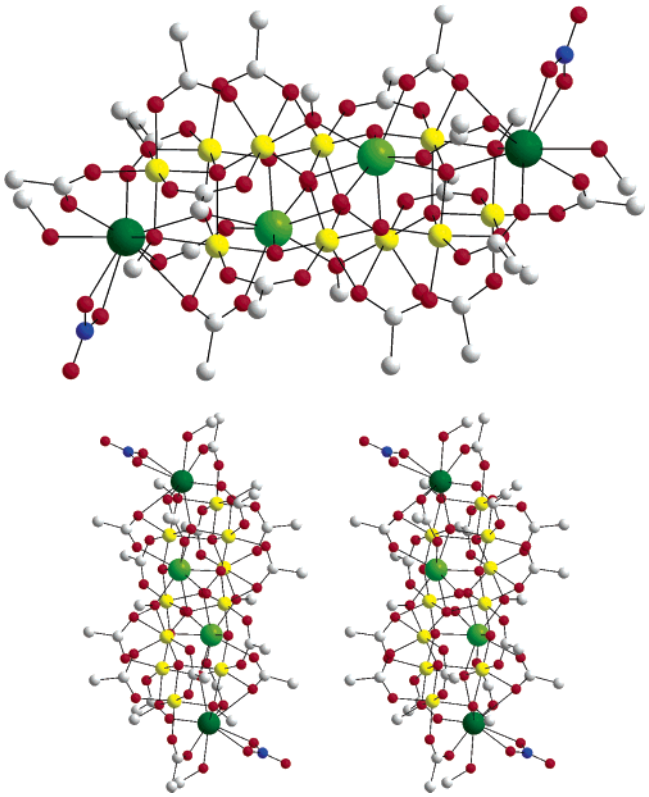

Figure 1. (Top) PovRay representation of the structure of **1**, with H atoms and the benzoate rings omitted for clarity except for the ipso C atoms: (bottom) a stereopair. Color scheme: Mn^{III} yellow; Ce^{III} dark green; Ce^{IV} light green; N dark blue; O red; C gray.

of 1:3 or 1:4 gave the same product. No isolable products were obtained when only MeCN was used. The preparation of **2** is summarized in eq 2.

$$5[Mn_4O_2(O_2CPh)_9(H_2O)]^- + 12Th(NO_3)_4{\cdot}3H_2O + 13H_2O \rightarrow 2[Th_6Mn_{10}O_{22}(OH)_2(O_2CPh)_{16}(NO_3)_2(H_2O)_8] + 44NO_3^- + 13PhCO_2H + 59H^+ + 20e^- \quad (2)$$

It is interesting that complex **1** contains 10 Mn^{III} atoms whereas **2** contains 10 Mn^{IV} atoms (vide infra), and this may partially be due to the greater quantities of MeOH in the former reaction, the alcohol being capable of acting as a reducing agent, as well as providing the MeO^- bridges in **1**. The other main difference between **1** and **2** is that the former contains both Ce^{III} and Ce^{IV}, whereas the latter contains only Th^{IV}, and this can be rationalized on the basis that Ce^{IV} is a stronger oxidizing agent than Th^{IV}. When the reactions were carried out in the presence of EtOH rather than MeOH, we were unable to isolate clean products.

Description of the Structures of 1 and 2. PovRay representations of **1** and **2** and their labeled cores are presented in Figures 1 and 2 (for **1**) and 3 and 4 (for **2**), respectively. Selected interatomic distances and angles for **1** and **2** are listed in Tables 2 and 3, respectively. For convenience, mention below of a particular atom will also implicitly include its symmetry-related partner.

Complex **1**·H_2O·4MeOH·6MeCN crystallizes in the monoclinic space group *C*2/*c* with the cluster lying on a center of symmetry. It contains 2 Ce^{III}, 2 Ce^{IV}, and 10 Mn^{III} atoms,

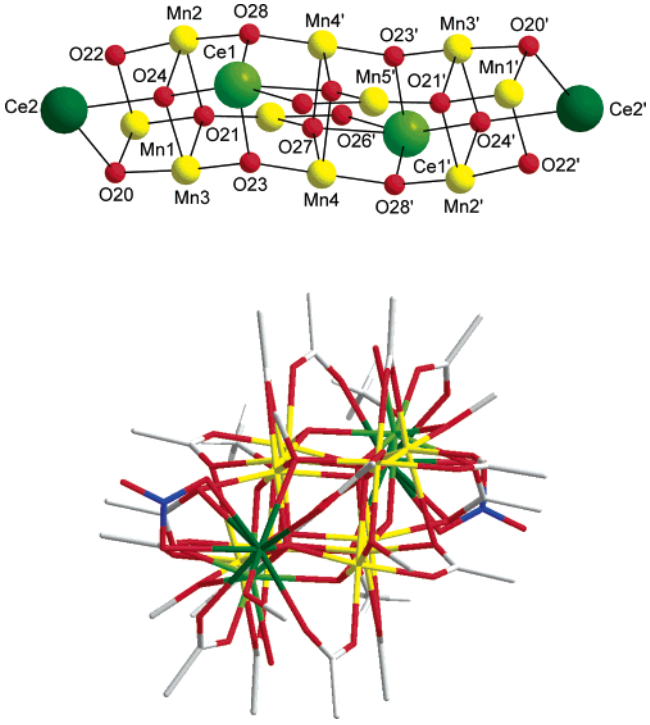

Figure 2. (Top) PovRay representation of the labeled core of **1**; (bottom) a stick representation from a viewpoint approximately down the tubular axis. Color scheme: Mn^{III} yellow; Ce^{III} dark green; Ce^{IV} light green; N dark blue; O red; C gray.

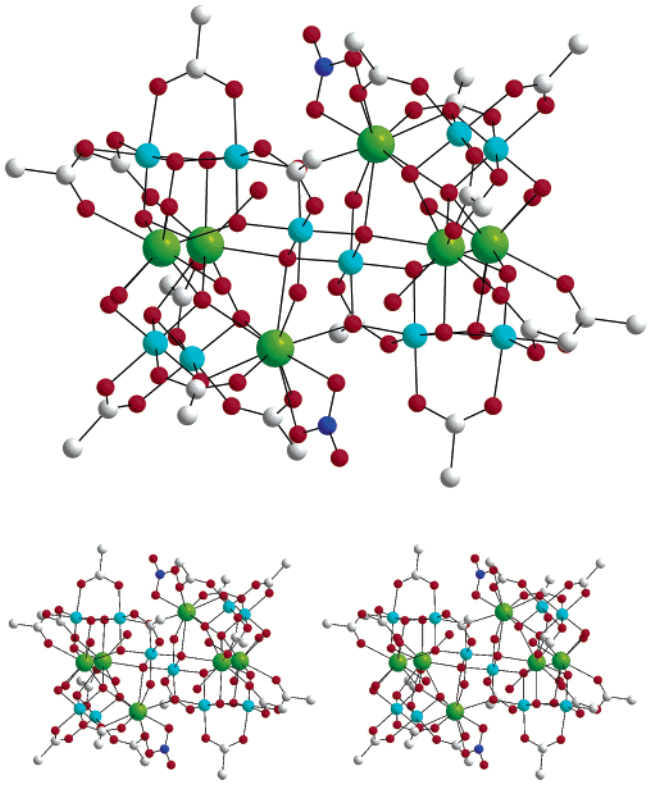

Figure 3. (Top) PovRay representation of the structure of **2** with H atoms and the benzoate rings omitted for clarity except for the ipso C atoms: (bottom) a stereopair. Color scheme: Mn^{IV} cyan; Th^{IV} light green; N dark blue; O red; C gray.

and these are held together by four μ_3-O^{2-}, six μ_4-O^{2-}, four μ_2-MeO^- (O22, O26), and two μ_3-MeO^- (O20) ions (Figure 2, top). The resulting $[Ce_4Mn_{10}O_{10}(OMe)_6]^{18+}$ core of **1** has

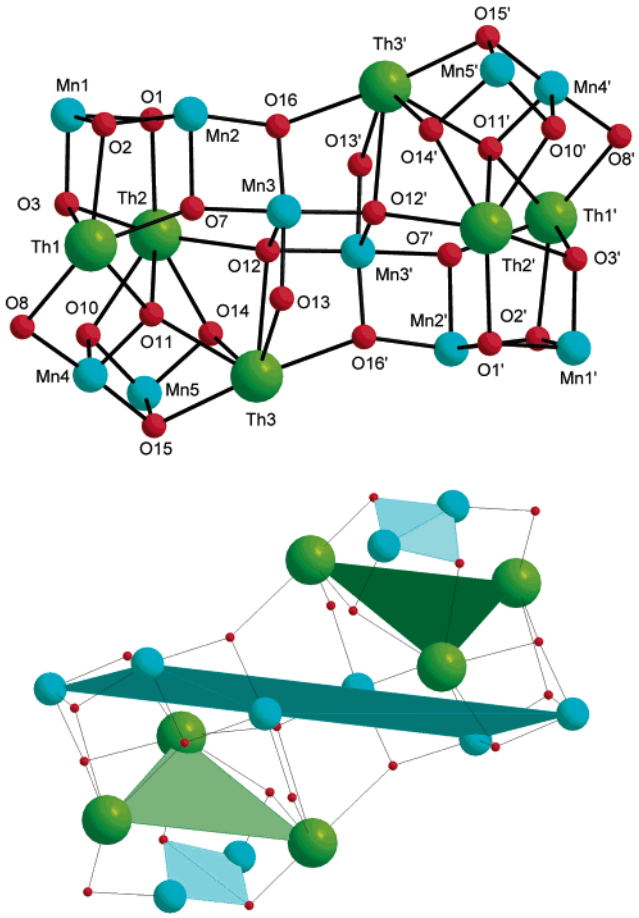

Figure 4. (Top) PovRay representation of the labeled core of **2**; (bottom) a representation emphasizing the 2:3:6:3:2 (Mn/Th/Mn/Th/Mn) layer structure. Color scheme: Mn^{IV} cyan; Th^{IV} light green; O red.

an approximately tubular structure, comprising a central $[Ce^{IV}_2Mn^{III}_4O_6(OMe)_2]$ unit attached at either end to a $[Ce^{III}Mn^{III}_3O_2(OMe)_2]$ distorted open-cubane unit (Figure 2); the latter would be a distorted (closed) cubane if the long, weak Ce2···O22 (2.966 Å) interaction is considered an additional bond. The tubular structure is 'sealed' at each end by a benzoate group bridging across the open face (Figure 2, bottom). Peripheral ligation is provided by 12 μ_2- and 4 μ_3-benzoate groups, a chelating nitrate group on each Ce^{III} atom (Ce2, Ce2′), a terminal H_2O molecule on each Ce^{IV} atom (Ce1, Ce1′), and a terminal MeOH group on each Ce^{III} atom. The doubly bridging O atoms of the four μ_3-benzoate goups in one case bridge a Mn^{III} pair (Mn4, Mn5) and in the other a Ce^{III}/Mn^{III} (Ce2/Mn3) pair. All the Mn atoms are six-coordinate with near-octahedral geometry. In contrast, the two Ce^{III} atoms (Ce2) are nine-coordinate (or 10-coordinate if Ce2···O22 is included) and the two Ce^{IV} atoms (Ce1) are eight-coordinate. The metal oxidation states and the protonation levels of O^{2-}, OMe^-, and H_2O groups were determined by bond valence sum (BVS) calculations,[18,19] inspection of metric parameters, charge balance considerations, and clear observation of Jahn−Teller (JT) distortion axes at all the Mn ions. The JT distortions all take the form of axial elongations, as is almost always the case for high-spin Mn^{III}, with JT elongated bonds being 0.1−0.3 Å longer than the other Mn^{III}−O bonds (∼1.8−2.0 Å). BVS values for O atoms of O^{2-}, OH^-, and H_2O groups are typically 1.8−2.0, 1.0−1.2, and 0.2−0.4, respectively, reflecting the non-inclusion of contributions from strong O−H bonds that are not usually observed with accuracy in X-ray studies. Participation of the group in hydrogen bonds will also affect these values. Oxygen BVS calculations are invaluable in high-nuclearity cluster chemistry, such as **1**, where the presence of, for example, a bridging O^{2-} vs OH^- may not be unequivocal from other considerations. For **1**, the BVS calculations clearly established the absence of bridging OH^- groups. The obtained Mn BVS values are shown in Table 4. The Ce^{III}−O and Ce^{IV}−O bonds are in the ranges 2.396−2.845 and 2.231−2.540 Å, respectively, both typical ranges for Ce^{III}−O and Ce^{IV}−O bonds in the literature.[18a,7,20] The corresponding BVS values clearly establish Ce1 and Ce2 as Ce^{IV} and Ce^{III}, respectively.[18]

Inspection of the crystal packing in **1**·H_2O·4MeOH·6MeCN reveals intermolecular hydrogen bonds between the nitrate and MeOH groups attached to Ce2 at each end of the molecule and the corresponding MeOH and nitrate groups attached to Ce2 of the neighboring molecule. This gives a one-dimensional, hydrogen-bonded chain with each chain connection comprising two O_2NO···HOMe hydrogen bonds with an O···O distance of 2.73 Å, typical for such an interaction. Since the groups involved are all attached to the paramagnetic Ce^{III} atoms, it is anticipated that they may result in noticeable intermolecular magnetic exchange interactions, albeit very weak ones since the pathways involve 4f orbital overlaps. We shall return to this point later (vide infra).

Complex **2**·10MeCN crystallizes in the triclinic space group $P\bar{1}$, with the cluster lying on an inversion center. It contains 10 Mn^{IV} and 6 Th^{IV} atoms held together by 4 μ_4-O^{2-}, 16 μ_3-O^{2-}, 2 μ-O^{2-}, and 2 μ-OH^- ions (Figure 3). Peripheral ligation around the resulting $[Th_6Mn_{10}O_{22}(OH)_2]^{18+}$ core is provided by 16 μ-$PhCO_2^-$ groups in their familiar syn, syn binding mode, a chelating nitrate group on Th3, and a total of 8 terminal H_2O groups on the other Th atoms, 3 on Th1, and 1 on Th2. The μ-benzoate groups bridge either Mn/Th or Mn/Mn pairs, none of them thus bridging Th_2 pairs. The latter are instead bridged by only oxide ions, and this is consistent with the known high oxophilicity of actinides. Indeed, Th2 and Th3 are each bound to six oxide ions and Th1 to five. In fact, it is noteworthy that there are so many oxide ions in the complex, a total of 22 oxides bridging 16 metal atoms. This is clearly a manifestation of the high oxidation state of +4 for all the Mn and Th atoms in **2**, and the resulting high preference for hard oxide ions as ligands. A closer examination of the centrosymmetric $[Th_6Mn_{10}O_{22}(OH)_2]^{18+}$ core (Figure 4)

(18) BVS values are 4.19 for Ce1 and 3.09 for Ce2. We employed a B_0 value of 0.37 Å, and $r_0 = 2.151$ Å for a Ce^{III}−O bond, and $r_0 = 2.09$ Å for a Ce^{IV}−O bond. (a) Roulhac, P. L.; Palenik, G. J. *Inorg. Chem.* **2003**, *42*, 118. (b) Brese, N. E.; O'Keeffe, M. *Acta. Crystallogr., Sect. B* **1991**, *47*, 192.

(19) (a) Brown, I. D.; Altermatt, D. *Acta. Crystallogr., Sect. B* **1985**, *41*, 244. (b) Liu, W.; Thorp, H. H. *Inorg. Chem.* **1993**, *32*, 4102. (c) Palenik, G. J. *Inorg. Chem.* **1997**, *36*, 4888.

(20) Tasiopoulos, A. J.; O'Brien, T.; Abboud, K. A.; Christou, G. *Angew. Chem., Int. Ed.* **2004**, *43*, 345.

Table 2. Selected Interatomic Distances (Å) and Angles (deg) for Complex **1**

Ce1−O28	2.231(6)	Ce2−O13	2.509(7)	Mn1−O10	2.051(7)	Mn1···Mn3	3.115(2)
Ce1−O14	2.240(8)	Ce2−O17	2.521(8)	Mn1−O22	2.072(8)	Mn1···Mn2	3.127(2)
Ce1−O23	2.267(6)	Ce2−O7	2.526(7)	Mn1−O20	2.115(6)	Ce1···Mn2	3.2907(15)
Ce1−O26	2.281(7)	Ce2−O19	2.615(8)	Mn4−O23	1.846(7)	Ce1···Mn4′	3.3165(15)
Ce1−O11	2.389(6)	Ce2−O20	2.620(7)	Mn4−O28′	1.867(7)	Ce1···Mn5	3.3774(17)
Ce1−O24	2.392(6)	Ce2−O18	2.629(7)	Mn4−O27′	1.999(6)	Ce2···Mn3	3.3653(18)
Ce1−O27	2.393(7)	Ce2−O12	2.845(8)	Mn4−O1′	2.031(7)	Ce2···Mn2	3.6257(16)
Ce1−O25	2.540(7)	Mn1-O21	1.855(6)	Mn4−O6	2.129(7)	Mn4···Mn4′	3.160(3)
Ce2−O16	2.396(9)	Mn1−O8	1.936(7)	Mn4−O27	2.278(6)	Mn4···Ce1′	3.3165(15)
Ce2−O24	2.425(7)	Mn1−O3	2.050(7)	Mn6···Mn7	2.812(2)	Ce2···O22	2.966(7)
O28−Ce1−O24	67.3(2)	Mn2−Ce1−Mn5	127.53(4)	Mn3−Mn1−Mn2	61.52(5)	Mn2−Mn3−Ce2	67.07(4)
O14−Ce1−O24	79.6(3)	O20−Ce2−Mn3	35.18(14)	Mn1−Mn2−Mn3	59.06(5)	Ce1−Mn3−Ce2	84.09(4)
O23−Ce1−O27	69.1(2)	Mn3−Ce2−Mn2	54.19(4)	Mn1−Mn2−Ce1	119.59(5)	Mn4′−Mn4−Ce1	59.66(5)
O26−Ce1−O27	65.0(2)	O22−Mn1−Mn2	37.05(19)	Mn2−Mn3−Ce1	61.22(4)	Ce1′−Mn4−Ce1	124.69(4)
Mn3−Ce1−Mn5	116.24(4)	O20−Mn1−Mn2	84.82(17)	Mn1−Mn3−Ce2	73.47(5)		

Table 3. Selected Interatomic Distances (Å) and Angles (deg) for Complex **2**

Th1−O3	2.376(14)	Th3−O16	2.397(13)	Mn1−O1	1.820(16)	Mn1···Mn2	2.695(4)
Th1−O7	2.393(12)	Th3−O15	2.424(11)	Mn1−O24	1.909(16)	Mn3···Mn3′	2.821(7)
Th1−O25	2.425(17)	Th3−O29	2.484(16)	Mn1−O21	1.945(17)	Mn2···Mn3	2.763(5)
Th1−O11	2.455(14)	Th3−O13	2.491(13)	Mn1−O22	1.984(14)	Mn4···Mn5	2.702(6)
Th1−O8	2.479(13)	Th3−O11	2.547(13)	Mn3−O7	1.828(14)	Th2···Mn5	3.362(3)
Th1−O6	2.501(19)	Th3−O17	2.584(15)	Mn3−O16′	1.831(13)	Th2···Mn1	3.420(4)
Th1−O2	2.514(14)	Th3−O18	2.59(2)	Mn3−O12	1.856(14)	Th2···Mn4	3.489(3)
Th1−O5	2.538(17)	Th3−O12	2.655(12)	Mn3−O12′	1.900(13)	Th3···Mn5	3.348(3)
Th1−O4	2.54(2)	Mn1−O3	1.802(13)	Mn3−O13	1.928(13)	Th3···Mn4	3.400(3)
Th3−O14	2.354(14)	Mn1−O2	1.807(15)	Mn3−O27	1.970(16)	Mn3···Th3′	3.460(3)
Th3−O32	2.384(16)						
O2−Th1−Mn4	133.4(4)	Mn1−Th1−Mn2	46.35(8)	Mn5−Th3−Mn4	47.19(10)	Mn2−Mn3−Th3	125.43(11)
Mn1−Th1−Mn4	104.58(10)	Mn4−Th1−Mn2	115.92(9)	Mn2−Mn1−Th1	70.16(11)	Mn3′−Mn3−Th2	77.49(12)
O3−Th1−Mn2	66.4(3)	O10−Th2−O1	140.0(5)	Mn2−Mn1−Th2	73.42(12)	Th3′−Mn3−Th2	106.87(9)
O11−Th1−Mn2	88.0(3)	Mn5−Th2−Mn4	46.40(10)	Th1−Mn1−Th2	69.06(7)	Th3−Mn3−Th2	63.24(5)
O8−Th1−Mn2	134.6(4)	Mn1−Th2−Mn4	100.92(9)	Mn1−Mn2−Mn3	127.94(15)	Mn3−O13−Th3	107.9(6)

Table 4. Bond Valence Sums for the Mn Atoms in **1** and **2**[a]

	1			**2**		
atom	Mn^{II}	Mn^{III}	Mn^{IV}	Mn^{II}	Mn^{III}	Mn^{IV}
Mn(1)	3.16	*2.89*	3.04	4.50	4.12	*4.33*
Mn(2)	3.27	*2.99*	3.14	4.33	3.96	*4.15*
Mn(3)	3.24	*2.96*	3.11	4.37	4.00	*4.20*
Mn(4)	3.20	*2.93*	3.09	4.38	4.00	*4.20*
Mn(5)	3.22	*2.95*	3.10	4.32	3.95	*4.15*

[a] The italicized value is the one closest to the charge for which it was calculated. The oxidation state of a particular atom can be taken as the nearest whole number to the italicized value.

Table 5. Bond Valence Sums[a] for Selected Oxygen Atoms in Complex **2**

atom	BVS	assignment	atom	BVS	assignment
O4	0.36	H_2O	O1	1.97	O^{2-}
O5	0.37	H_2O	O15	2.16	O^{2-}
O6	0.40	H_2O	O12	2.06	O^{2-}
O9	0.35	H_2O	O16	2.06	O^{2-}
O13	1.03[b]	O^{2-}	O14	1.87	O^{2-}
O8	1.05	OH^-	O10	2.07	O^{2-}
O2	2.30	O^{2-}	O3	1.96	O^{2-}
O11	1.93	O^{2-}	O7	1.91	O^{2-}

[a] BVS values for O atoms of O^{2-}, OH^-, and H_2O groups are typically 1.8−2.0, 1.0−1.2, and 0.2−0.4, respectively. [b] The abnormally low value for an oxide ion is assigned to hydrogen bonding. See the text for details.

reveals that each half can be described as two distorted [$Mn_2Th_2O_4$] cubane units sharing a common vertex (Th2). The two cubanes comprise {Mn1, O1, Mn2, O2, Th1, O7, O3, Th2} and {Th2, O14, Mn5, O10, Mn4, O15, Th3, O11} and are also connected by μ-OH^- oxygen atom O8, which is the only hydroxide ion in each half of the cluster (Figure 4, top). Each of the two dicubane units is then linked by three oxides (O12, O13, O16, and their symmetry partners) to central Mn atoms Mn3 and Mn3′. All the Mn atoms are six-coordinate with near-octahedral geometry. In contrast, four Th ions (Th1, Th2) are nine-coordinate, and the remaining two (Th3) are 10-coordinate. The metal oxidation states and the protonation level of O^{2-}, OH^-, and H_2O groups were determined by BVS calculations,[21] inspection of metric parameters, and charge balance considerations. The BVS values for the Mn ions are listed in Table 4, and it can be seen that all the Mn atoms in **2** are Mn^{IV}. The Mn−O bond distances in **2** are in the range 1.802−2.027 Å, consistent with the Mn^{IV} oxidation level. Similarly, all the Th atoms were concluded by BVS calculations to be Th^{IV},[21] and the Th−O bond range of 2.354−2.655 Å is indeed typical of Th^{IV}−O bonds in the literature.[22] The O BVS calculations[19] (Table 5) suggested 20 O^{2-} and 4 OH^- ions, which was unexpected and in conflict with the overall charge balance calculated from the metal oxidation states. The conflict was tracked down to μ-O atom O13, which has a BVS of 1.03, suggestive of an OH^- ion. However, this was concluded to be in reality an O^{2-} ion whose abnormally low BVS is the result of its participation in two strong O···H−O hydrogen bonds with two terminal H_2O groups, O6 and O9′, on Th1

(21) r_0 = 2.167 Å and B_0 = 0.37 Å for a Th^{IV}−O bond. (b) Brese, N. E.; O'Keeffe, M. *Acta. Crystallogr., Sect. B* **1991**, *47*, 192. BVS values gave the range 4.23−4.31 for the Th ions of **2**.

(22) Kim, J.; Norquist, A. J.; O'Hare, D. *J. Am. Chem. Soc.* **2003**, 125, 12688. (b) Sullens, T. A.; Albrecht-Schmitt, T. E. *Inorg. Chem.* **2005**, *44*, 2282.

and Th2′, respectively (O13···O6 = 2.796 Å; O13···O9′ = 2.834 Å). This lengthens the corresponding Mn−O13 and Th−O13 bonds and leads to a lower BVS for O13. Thus, O13 is indeed an O^{2-} ion, consistent with charge neutrality for the complete molecule.

The core of **2** can be considered as consisting of alternating layers of Th and Mn atoms, as emphasized in Figure 4 (bottom). The metal topology can be described as five layers with a 2:3:6:3:2 pattern of metal content. The Th atoms thus occur as two Th_3 isosceles triangles, the Th1···Th2 and Th2···Th3 distances (3.829 Å) being significantly shorter than the Th1···Th3 (4.808 Å) distance. In fact, one can also describe the core of **1** as consisting of layers, in this case seven layers of CeMn and Mn_2 in an alternating A:B:A:B:A:B:A arrangement. There are no significant intermolecular interactions in **2**.

The Th_6Mn_{10} complex **2** is the largest mixed transition metal/actinide complex to date and the first Th/Mn cluster. Currently there are metal−organic frameworks[22a] and organically templated thorium complexes[23] known, and the largest molecular Th complex is Th_6.[24] Similarly, the Ce_4Mn_{10} complex **1** is the largest mixed-metal Ce/Mn cluster and the first 3d/4f cluster with mixed-valency in its lanthanide component. $Ce^{IV}Mn^{III}$ and $Ce^{IV}Mn^{IV}$ clusters have both been reported previously, but this is the first to contain both oxidation states of Ce. Note that both of these complexes contain heterometallic cubane units containing high-oxidation-state (III, IV) Mn ions, which is also of relevance to the lanthanide-substituted Mn_4Ca site of the water oxidizing complex of photosynthesis,[3,4] where the corresponding Mn_3-Ln cubane may be forming. Such Mn-containing heterometallic cubanes were unknown in inorganic chemistry until seen for the first time in mixed Mn/lanthanide[8a] and Mn/Ca complexes reported recently.[3b]

DC Magnetic Susceptibility Studies. Solid-state, variable-temperature magnetic susceptibility measurements were performed on vacuum-dried microcrystalline samples of complexes **1**·$4H_2O$ and **2**, which were suspended in eicosane to prevent torquing. The dc magnetic susceptibility (χ_M) data were collected in the 5.0−300 K range in a 0.1 T magnetic field, and are plotted as $\chi_M T$ vs T in Figure 5.

For **1**·$4H_2O$, $\chi_M T$ decreases steadily from 34.38 $cm^3\ mol^{-1}$ K at 300 K to 10.26 $cm^3\ mol^{-1}$ K at 5.0 K, which indicates the presence of predominantly antiferromagnetic exchange interactions within the molecule. The calculated $\chi_M T$ for a $Ce^{III}_2Ce^{IV}_2Mn^{III}_{10}$ cluster with non-interacting metal ions is 31.6 $cm^3\ mol^{-1}$ K, taking $g_{Mn} = 2.0$ and $g_{Ce} = 0.86$ (free Ce^{III} ion, f^1, $S = 1/2$, L = 3, $^2F_{5/2}$, $\chi_M T = 0.81$ $cm^3\ mol^{-1}$ K). For **2**, $\chi_M T$ decreases only very slightly from 17.54 $cm^3\ mol^{-1}$ K at 300 K down to ∼25 K and then decreases more rapidly with decreasing temperature to 7.41 $cm^3\ mol^{-1}$ K at 5.0 K. The 300 K value is slightly lower than the 18.75 $cm^3\ mol^{-1}$ K value expected for a cluster of 10 non-interacting Mn^{IV} ions (Th^{IV} is diamagnetic), again indicating the presence of dominant antiferromagnetic exchange interactions within

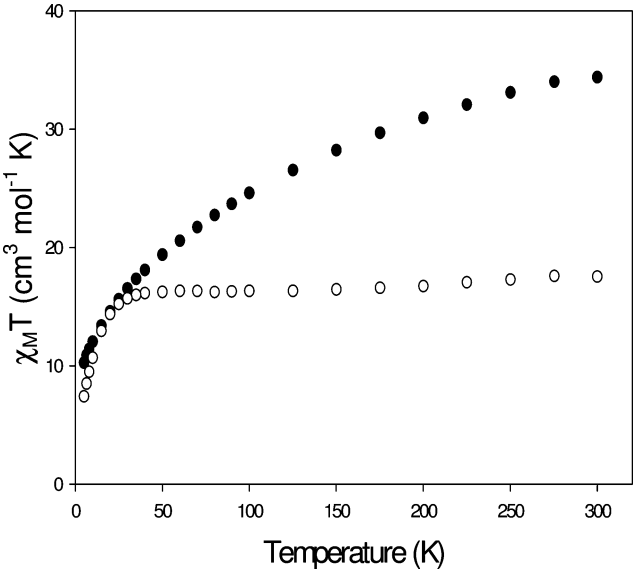

Figure 5. Plots of $\chi_M T$ vs T for complexes **1**·$4H_2O$ (●) and **2** (○).

2. The $\chi_M T$ values at 5.0 K indicate relatively small ground state spins for **1** and **2**.

Complex **1** contains 10 Mn^{III} ($S = 2$) and 2 Ce^{III} ($S = {}^1/_2$) spin carriers and therefore has total spin values in the range 0−21. Similarly, with 10 Mn^{IV} ($S = {}^3/_2$) atoms, complex **2** has total spin values in the range 0−15. Owing to the size and low symmetry of the molecules, a matrix diagonalization method to evaluate the various pairwise exchange parameters (J_{ij}) between metals M_i and M_j in the complexes is very onerous. In addition, application of the equivalent operator approach based on the Kambe vector coupling method[25] is not possible. Therefore, we focused only on identifying the ground state spin S values and the zero-field splitting D parameters for **1**·$4H_2O$ and **2**; these would in any case dominate the ultra-low-temperature studies we subsequently performed (vide infra). Hence, magnetization (M) data were collected in magnetic fields up to 7 T and in the temperature range 1.8−10 K, and these are plotted as reduced magnetization ($M/N\mu_B$) versus H/T in Figure 6. The data were fit, using the program MAGNET,[15] by diagonalization of the spin Hamiltonian matrix assuming only the ground state is populated, incorporating axial anisotropy ($D\hat{S}_z^2$) and Zeeman terms, and employing a full powder average. Thus, the complexes are modeled for the magnetization fit as a 'giant spin' with Ising-like anisotropy. The corresponding Hamiltonian is given by eq 3, where μ_B is the Bohr magneton, $\hat{S}_z$ is the easy-axis spin operator, g is the electronic g factor, μ_0 is the vacuum permeability, and H is the applied field.

$$H = D\hat{S}_z^{\,2} + g\mu_B\mu_0\hat{S}\cdot H \qquad (3)$$

The last term in eq 3 is the Zeeman energy associated with the applied magnetic field.

Preliminary attempts to fit the data collected up to 7 T were unsuccessful, which was as anticipated given the high

(23) Kim, J.; Norquist, A. J.; O'Hare, D. *Chem. Commun.* **2002**, 2198.

(24) Barnhart, D. M.; Butcher, R. J.; Clark, D. L.; Gordon, J. C.; Watkin, J. G; Zwick, B. D. *New J. Chem.* **1995**, *19*, 503.

(25) Kambe, K. *J. Phys. Soc. Jpn.* **1950**, *48*, 15.

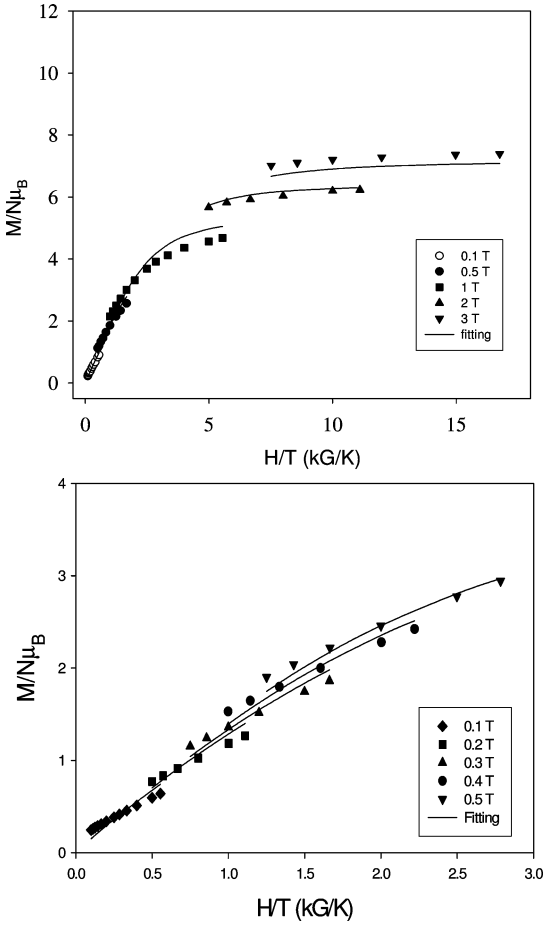

Figure 6. Magnetization (M) vs field (H) and temperature (T) data, plotted as reduced magnetization ($M/N\mu_B$) vs H/T, for (top) complex **1**·4H_2O at applied fields of 0.1−3.0 T and in the 1.8−10 K temperature range; and (bottom) complex **2** at applied fields of 0.1−0.5 T and in the 1.8−10 K temperature range. The solid lines are the fit of the data; see the text for the fit parameters.

nuclearity of the complexes and the many constituent pairwise exchange interactions; most if not all of the latter are expected to be antiferromagnetic, and some of them are undoubtedly very weak. Competing antiferromagnetic interactions within the many triangular M_3 subunits of the structures will also lead to spin frustration effects. The expected net result is a high density of low-lying (relative to kT) excited states in **1**·4H_2O and **2**. Since many of these would be expected to have an S value greater than that of the ground state, the application of a large dc field will cause problems as M_S levels of excited states under the influence of the field will approach in energy and even cross with those of the ground state. This would lead to poor fits of the magnetization data, since the fitting model assumes only the ground state is populated. To avoid this, we used in the fits only data collected at low dc fields in order to obtain estimates of S. For complex **1**·4H_2O, the fit (solid lines in Figure 6 (top)) using data in the 0.1−3.0 T range gave $S = 4$, $D = -0.57(2)$ cm^{-1} and $g = 2.09(1)$. This must be considered only an approximation since it ignores first-order spin−orbit effects from the Ce^{III} ions, and this is also undoubtedly the cause of the high g value. For complex **2**, there are no such spin−orbit effects from the Th^{IV} (f^0) atoms but still we could not obtain an acceptable fit even if we used only data collected in the 0.1−0.5 T range. We believe this must be due to a particularly high density of low-lying excited states, and this is supported by the ac studies (vide infra). The best (but still poor) fit was with $S = 4$, $D = -0.81(16)$ cm^{-1}, and $g = 1.85(2)$, shown as the solid lines in Figure 6 (bottom), and this is also unacceptable on the basis of the D value, which is unreasonably high for a molecule containing only near-isotropic Mn^{IV} atoms. Thus, the magnetization fit was taken as indicating merely a rough value of $S = 3-5$, and it was clear that a better means of obtaining a reliable value for the ground state S of **2** was necessary. For the latter, we turned to ac susceptibility methods.[5f,11,26] In addition, the ac methods would allow us to ascertain if either complex **1** or **2** might be a new addition to the growing family of SMMs.

AC Magnetic Susceptibility Studies. Alternating-current magnetic susceptibility studies were performed on vacuum-dried microcrystalline samples of **1**·4H_2O and **2** in the temperature range 1.8−10 K with a 3.5 G ac field oscillating at frequencies in the 5−1000 Hz range. The ac susceptibility experiment probes the dynamics of the relaxation of the magnetization (magnetic moment) vector of a system. The in-phase (χ_M') component of the ac susceptibility of **1**·4H_2O and **2** is shown as $\chi_M'T$ vs T in Figures 7 (top) and 8, respectively. The in-phase $\chi_M'T$ signal serves as a useful tool for determining (or confirming) the ground state spin of a molecule, since it avoids the Zeeman complications mentioned earlier arising from low-lying excited states in an applied dc field. The $\chi_M'T$ extrapolated, from a temperature high enough to avoid the effects of any weak intermolecular interactions or slow relaxation, to 0 K (where only the ground state would be populated) should thus be in agreement with $\chi_M'T = (g^2/8)S(S+1)$, where S is the ground state spin, for complex **2**. However, for complex **1**, the analysis is more complicated because L and J become increasingly important due to the presence of Ce^{III} ions.

For **1**·4H_2O (Figure 7, top), the in-phase $\chi_M'T$ data above 3 K increase with increasing temperature, in agreement with the presence of low-lying excited states with spin greater than that of the ground state, and spin−orbit effects from the Ce(III) ions. Extrapolation to 0 K from above 3 K gives a value of ∼9.2 cm^3 mol^{-1} K, which is consistent with $S \approx 4$ if the spin−orbit contributions from Ce^{III} are considered small; the latter conclusion seems reasonable given that even the free Ce^{III} ion has a magnetic moment of only 0.81 cm^3 mol^{-1} K, and there will be some quenching of its orbital angular momentum within **1**. For **2** (Figure 8), the $\chi_M'T$ data increase very rapidly with increasing temperature, more than doubling over ∼8 K from 6.80 cm^3 mol^{-1} K at 1.8 K to 14.30 cm^3 mol^{-1} K at 10 K. This is steeper than the rise for **1**·4H_2O (note the difference in scales between the vertical axes in Figures 7 (top) and 8) and is consistent with a higher density of low-lying excited states in **2** compared with **1**·4H_2O. This is also consistent with the failure to obtain a

(26) (a) King, P.; Wernsdorfer, W.; Abboud, K. A.; Christou, G. *Inorg. Chem.* **2005**, *44*, 8659. (b) Foguet-Albiol, D.; Abboud, K. A.; Christou, G. *Chem. Commun.* **2005**, 4282.

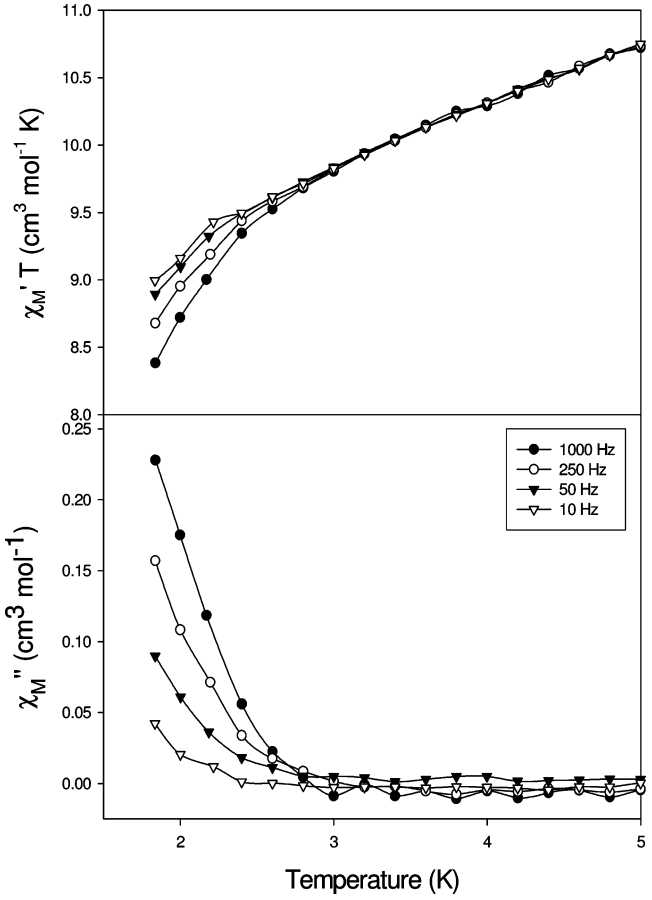

Figure 7. Ac susceptibility of complex **1** in a 3.5 G field oscillating at the indicated frequencies. (Top) In-phase signal (χ_M') plotted as $\chi_M'T$ vs T: (bottom) out-of-phase signal χ_M'' vs T.

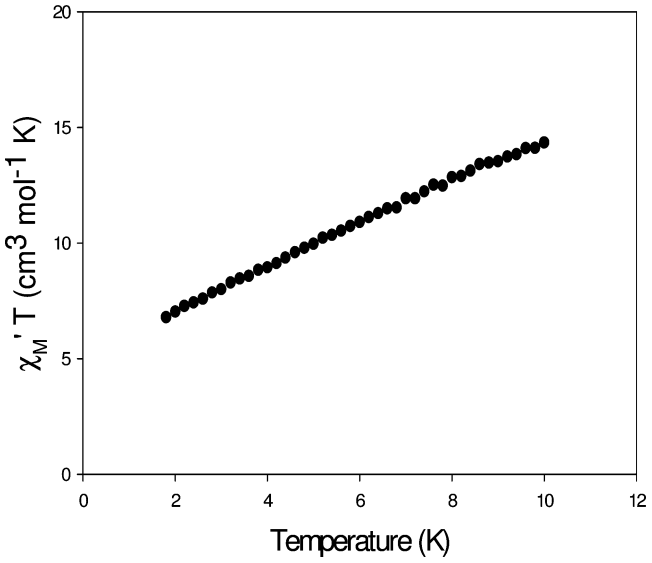

Figure 8. Plot of the in-phase ac susceptibility signals, $\chi_M'T$ vs T for complex **2**.

good fit of the dc magnetization data for **2**, even using only low-field data. Nevertheless, extrapolation of the $\chi_M'T$ to 0 K, where only the ground state would be populated, gives a value of $\sim$5.2 cm^3 mol^{-1} K indicative of an $S = 3$ ground state and $g \approx 1.86$. Note that $S = 2$, 3, and 4 ground states would give values of $\chi_M'T$ of 3.0, 6.0, and 10.0 cm^3 mol^{-1} K for $g = 2$ (slightly less for $g < 2$), clearly identifying $S = 3$ as the true ground state of **2**.

The frequency-dependent decrease in the $\chi_M'T$ of **1**·4H_2O below 3 K suggested there would also be a corresponding frequency-dependent out-of-phase (χ_M'') signal, and this was indeed observed (Figure 7, bottom), or rather the tails of frequency-dependent peaks whose maxima lie below 1.8 K, the operating limit of our SQUID susceptometer. An out-of-phase (χ_M'') ac susceptibility signal is observed when the rate at which the magnetization of a system relaxes is close to the operating frequency of the ac field. At low enough temperature, when kT is lower than the relaxation barrier, the magnetization vector cannot relax fast enough to keep in-phase with the oscillating field, and a frequency-dependent χ_M'' signal will be observed, together with a concomitant decrease in the in-phase $\chi_M'T$ signal. Such frequency-dependent signals are characteristic of superparamagnets in traditional magnetism and also of SMMs. This (Figure 7, bottom) suggests complex **1** might be an SMM, but χ_M'' signals do not by themselves prove it since intermolecular interactions and phonon bottlenecks can also give such signals.[27] It will be important for the discussion that follows below to note that we repeated the ac studies with a sample of crystals of **1**·H_2O·4MeOH·6MeCN still wet with mother liquor, and we saw the same χ_M'' signals as those for dried **1**·4H_2O in Figure 7, bottom. Complex **2** exhibited no out-of-phase signals.

Hysteresis Studies below 1.8 K. In order to confirm whether complex **1** is a new SMM, we performed magnetization vs applied dc field measurements on single crystals of **1**·H_2O·4MeOH·6MeCN at temperatures down to 0.04 K using a micro-SQUID apparatus.[16] The observation of hysteresis loops in such studies represents the diagnostic property of a magnet, including SMMs and superparamagnets below their blocking temperature (T_B). The observed magnetization responses for **1**·H_2O·4MeOH·6MeCN are shown in Figure 9 (top) at a fixed dc field sweep-rate of 0.035 T/s and at temperatures in the range of 0.04−5.0 K and (bottom) at 0.04 K and in the sweep-rate range 0.035−0.280 T/s. Some minor hysteresis was observed but with a very narrow coercivity that did not change noticeably with either decreasing T or increasing scan rate in the 0.04−5 K, and 0.035−0.280 T/s ranges. This is clearly not the superparamagnet-like behavior expected of an SMM, and the small coercivity is assigned as due primarily to a phonon bottleneck rather than a real, single-molecule barrier to magnetization relaxation, i.e., an artifact of the depletion of the appropriate energy phonons required to assist in the magnetization relaxation via a two-phonon Orbach process. However, the tiny hysteresis at 0.04 K appears to be real, and this is assigned as due to the weak intermolecular interactions propagated by the intermolecular hydrogen bonds between the chelating nitrate and MeOH groups on one molecule and the corresponding MeOH and nitrate groups on each neighboring molecule, as described above, giving one-

(27) Chakov, N. E.; Wernsdorfer, W.; Abboud, K. A.; Christou, G. *Inorg. Chem.* **2004**, *43*, 5919.

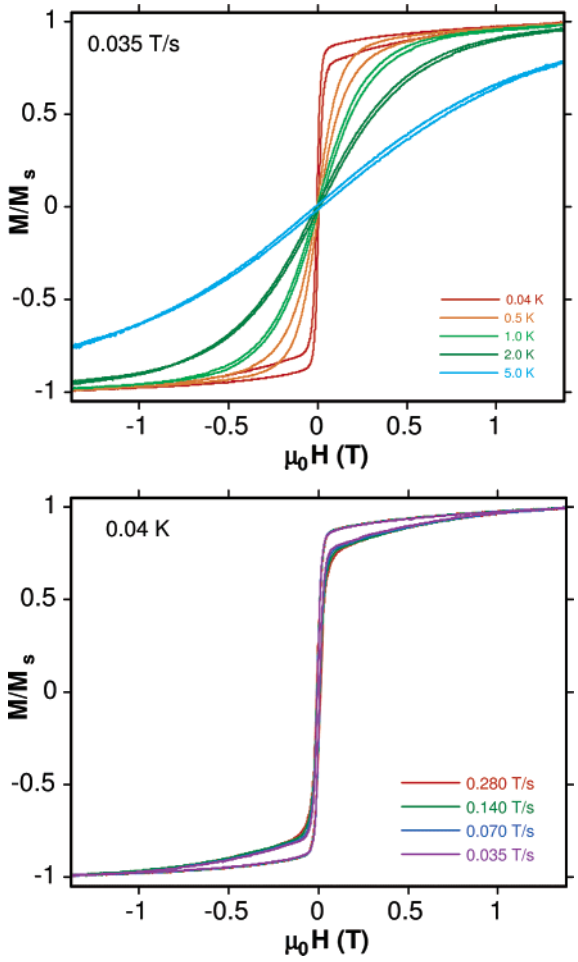

Figure 9. Magnetization (M) vs applied magnetic field (H) hysteresis loops for **1** at the indicated temperatures and a fixed-field sweep rate of 0.035 T/s (top), and at the indicated-field sweep rates and a fixed temperature 0.04 K (bottom). The magnetization is normalized to its saturation value, M_S.

dimensional chains. These would be expected to be very weak, particularly since they involve the Ce^{III} ions because lanthanides are known to always give weak exchange interactions because of the 'buried' nature of their 4f orbitals. We therefore conclude that any real hysteresis is only evident at 0.04 K and that this is in any case not due to single-molecule properties but to intermolecular interactions. Thus, complex **1**·H_2O·4MeOH·6MeCN is not an SMM.

Conclusions

We have described two new developments within our program directed toward the preparation and study of high-nuclearity transition metal clusters of paramagnetic metal ions. Complex **1** is the largest mixed-metal Ce/Mn cluster and the first 3d/4f cluster with mixed valency in its lanthanide component, while complex **2** is the first Th/Mn cluster and the largest mixed transition metal/actinide cluster to date. The latter point suggests **2** might be the prototype of a rich new area of mixed 3d/5f cluster chemistry with carboxylates and other ligand types. The next largest member of this family is a $Cu_2Mo_{12}U$ polyoxometallate.[28] Indeed, polyoxometallates are relatively common in actinide chemistry, but in contrast, there are only very few structurally characterized mixed-metal carboxylate complexes containing actinides, and these are small nuclearity species.

Magnetic characterization of complexes **1** and **2** has been carried out, and they are both relatively low-spin complexes with spin values of $S \approx 4$ and $S = 3$ for **1** and **2**, respectively. Ac susceptibility studies on **1**·H_2O·4MeOH·6MeCN still wet with mother liquor and dried **1**·$4H_2O$ both display frequency-dependent decreases below 3 K in the in-phase susceptibility and concomitant frequency-dependent out-of-phase signals. However, magnetization vs dc field sweeps down to 0.04 K revealed true (but very slight) hysteresis only at 0.04 K, which we assign to the intermolecular hydrogen bonding seen in the crystal structure. We conclude that there is an absence of any significant single-molecule barrier (vs kT) to magnetization relaxation. Thus, complex **1** is not an SMM. The clear observation of the out-of-phase χ_M'' ac signals below 3 K is thus surprising. The tiny barrier responsible for the almost insignificant hysteresis at 0.04 K is not expected to give χ_M'' signals at the higher temperatures up to 3 K. Typically, complexes that give significant tails of ac χ_M'' signals at >1.8 K then reveal clear hysteresis in dc magnetization sweeps assignable to an SMM with blocking temperatures of at least ~0.6 K or more. Nor can the answer be due to whether the sample was used wet with mother liquor or first dried. We have certainly seen in the past that the latter sometimes causes significant differences in the relaxation barrier,[26a,29,30] for example, wet crystals showing no χ_M'' signals down to 1.8 K but dried solid showing strong ones at >1.8 K.[29] For complex **1**, in contrast, wet and dried samples give essentially identical χ_M'' signals, so it is valid to compare the ac data in Figure 7 with the single-crystal data in Figure 9. Thus, we cannot offer an unequivocal explanation of the origin of the χ_M'' signals, except to state the obvious that it must be due to a combination of factors such as intermolecular interactions, phonon bottlenecks, and perhaps other contributions. Note that the groups involved in the hydrogen bonds between neighboring molecules are attached to metal ions and thus would not be expected to be lost on drying, as confirmed by the elemental analysis of dried material. We thus do not anticipate any significant change to the intermolecular hydrogen bonds on drying. This is consistent with the observation that wet and dried samples give essentially identical χ_M'' signals. In any case, much more important is the overall conclusion from the combined results of this study that, as we have stated before, the appearance of χ_M'' signals is necessary but not sufficient proof of a SMM. Complex **1** is now another example of this important caveat.[27]

(28) Petrukhina, M. A.; Sergienko, V. S.; Sadikov, G. G.; Tat'yanina, I. V.; Torchenkova, E. A. *Koord. Khim. (Russ.) (Coord. Chem.)* **1990**, *16*, 354.
(29) Boskovic, C.; Brechin, E. K.; Streib, W. E.; Folting, K.; Bollinger, J. C.; Hendrickson, D. N.; Christou, G. *J. Am. Chem. Soc.* **2002**, *124*, 3725.
(30) (a) Tasiopoulos, A. J.; Wernsdorfer, W.; Abboud, K. A.; Christou, G. *Angew. Chem., Int. Ed.* **2004**, *43*, 6338. (b) Tasiopoulos, A. J.; Wernsdorfer, W.; Abboud, K. A.; Christou, G. *Inorg. Chem.* **2005**, *44*, 6324.

Acknowledgment. We thank the National Science Foundation for support of this work.

Supporting Information Available: X-ray crystallographic data in CIF format for complexes **1**·H_2O·4MeOH·6MeCN and **2**·10MeCN. This material is available free of charge via the Internet at http://pubs.acs.org.

IC061946Y